Quasiequilibrium sequences of synchronized and irrotational binary neutron stars in general relativity. III. Identical and different mass stars with $\gamma = 2$

Keisuke Taniguchi

Department of Earth Science and Astronomy, Graduate School of Arts and Sciences,
University of Tokyo, Komaba, Meguro, Tokyo 153-8902, Japan

Eric Gourgoulhon

Laboratoire de l'Univers et de ses Théories, FRE 2462 du CNRS,
Observatoire de Paris, F-92195 Meudon Cedex, France
(Dated: 19 September 2002)

We present the first computations of quasiequilibrium binary neutron stars with different mass components in general relativity, within the Isenberg-Wilson-Mathews approximation. We consider both cases of synchronized rotation and irrotational motion. A polytropic equation of state is used with the adiabatic index $\gamma = 2$. The computations have been performed for the following combinations of stars: $(M/R)_{\infty,\,\text{star 1}}$ vs. $(M/R)_{\infty,\,\text{star 2}} =$ 0.12 vs. (0.12, 0.13, 0.14), 0.14 vs. (0.14, 0.15, 0.16), 0.16 vs. (0.16, 0.17, 0.18), and 0.18 vs. 0.18, where $(M/R)_{\infty}$ denotes the compactness parameter of infinitely separated stars of the same baryon number. It is found that for identical mass binary systems there is no turning point of the binding energy (ADM mass) before the end point of the sequence (mass shedding point) in the irrotational case, while there is one before the end point of the sequence (contact point) in the synchronized case. On the other hand, in the different mass case, the sequence ends by the tidal disruption of the less massive star (mass shedding point). It is then more difficult to find a turning point in the ADM mass. Furthermore, we find that the deformation of each star depends mainly on the orbital separation and the mass ratio and very weakly on its compactness. On the other side, the decrease of the central energy density depends on the compactness of the star and not on that of the companion.

PACS numbers: 04.25.Dm, 04.40.Dg, 97.60.Jd, 97.80.-d

I. INTRODUCTION

Coalescing binary neutron stars are expected to be one of the most promising sources of gravitational waves that could be detected by the ground based, kilometer size laser interferometers such as the Laser Interferometric Gravitational wave Observatory (LIGO), VIRGO, GEO600, and TAMA300 [1], and also are considered as one of candidates of gamma-ray burst source [2].

Due to the emission of gravitational radiation, binary neutron stars decrease their orbital separations and finally merge. When discussing the evolution of the system, it is convenient to separate it into three phases. The first one is the *inspiraling phase* in which the orbital separation is much larger than the neutron star radius, and the post-Newtonian (PN) expansion constitutes an excellent approximation. Recently, two groups succeeded in deriving the 3PN equation of motion of point-mass binary systems [3, 4], and the equivalence of the results between these groups is shown in [5, 6]. The second stage is the *intermediate phase* in which the orbital separation becomes only a few times larger than the radius of a neutron star, so that hydrodynamics as well as general relativity play an important role. In this phase, since the shrinking time of the orbital radius due to the emission of gravitational waves is still larger than the orbital period, it is possible to approximate the state as quasiequilibrium. The final stage is the *merging phase* in which the two stars coalesce dynamically. As in the intermediate phase, since hydrodynamics as well as general relativity play an important role, fully relativistic hydrodynamical treatments are required in this phase which therefore pertains to the field of numerical relativity. The first successful computations of the evolution of binary neutron stars from their innermost stable circular orbits (ISCO) to black hole or massive neutron star formation have been performed by Shibata and Uryu [7, 8]. Other efforts are presented in [9, 10].

The present article belongs to the series of works [11], [12] (hereafter Paper I), [13] (hereafter Paper II), [14], devoted to the intermediate phase. This stage is interesting because we may get informations about equation of state of neutron stars through the ISCO [15]. Furthermore, it is important from a numerical point of view since it provides initial data for the dynamical simulation in the merging phase [7, 8]. Then numerous theoretical efforts are devoted in this phase

---

[1] For TAMA300, data taking has started in summer 1999, and the first results of the data analysis have been published [1].

including (semi-)analytic Newtonian [16, 17] and post-Newtonian [18, 19, 20, 21] approaches and numerical Newtonian [13, 14, 22, 23, 24], post-Newtonian [25], and general relativistic [11, 12, 26, 27, 28, 29, 30, 31, 32] ones. Among these studies, we concentrate on numerical computations in the general relativistic framework. Kochaneck [33] and Bildsten and Cutler [34] have shown that the gravitational-radiation driven evolution is too rapid for the viscous forces to synchronize the spin of each neutron star with the orbit as they do for ordinary stellar binaries. Rather, the viscosity is negligible and the fluid velocity circulation (with respect to some inertial frame) is conserved in these systems. Provided that the initial spins are not in the millisecond regime, this means that close binary configurations are well approximated by zero vorticity (i.e. *irrotational*) states. Formulations for irrotational binaries in general relativity have been developed by several authors [35, 36, 37, 38] (see Appendix A of Paper I for a comparison between them). In addition to the quasiequilibrium and irrotational assumptions, we use the approximation of a conformally flat spatial 3-metric, introduced by Isenberg [39] and Wilson and Mathews [40] (hereafter IWM approximation; see Sec. IV.C of [41] and Sec. III.A of Paper I for a discussion).

Until now, several groups have produced quasiequilibrium configurations of binary neutron stars, as listed above. Among them, there are results for synchronized [26, 27] and irrotational [11, 12, 28, 29, 30] rotation states in the general relativistic framework, within the IWM approximation, and those for synchronized one within some axisymmetric approximation [31, 32]. However they all deal with *identical* star binaries and calculations for *different* mass binary system in general relativity have not been performed yet (in Newtonian theory they have been performed in the synchronized case [14, 23], and recently in the irrotational one [14]).

We will present here the first numerical results of relativistic binary systems composed of different mass stars. In addition, we give results for systems of identical stars which extend those already presented in Paper I. As a first step in the study of different mass systems, we restrict our computations to a polytropic equation of state, with the adiabatic index $\gamma = 2$.

The plan of the article is as follows. A brief overview of our method is given in Sec. II. In Sec. III, new tests of the numerical code are shown, which were not given in Papers I and II. We present the numerical results in Sec. IV, and discuss them in Sec. V. Finally Sec. VI is devoted to the summary.

Throughout this article, we adopt geometrical units: $G = c = 1$, where G and c denote the gravitational constant and speed of light, respectively.

II. METHOD

The reader is referred to Secs. II, III, and IV of Paper I for the complete set of equations governing perfect fluid binary stars under the assumption of quasiequilibrium and conformally flat spatial metric, as well as the numerical method which we use. We simply give here some outline of the method.

Let us summarize the assumptions expressed in Sec. I. The first one is *quasiequilibrium*, resulting from the fact that the time scale of orbital shrinking is larger than that of the orbital revolution until the ISCO. This assumption is taken into account by demanding that the spacetime is endowed with a *helical Killing vector*

$$\boldsymbol{l} = \frac{\partial}{\partial t} + \Omega \frac{\partial}{\partial \varphi}, \tag{1}$$

where Ω is the orbital angular velocity and the vectors $\partial/\partial t$ and $\partial/\partial \varphi$ are associated with the time coordinate t and the azimuthal coordinate φ of an asymptotical inertial observer. The second assumption regards the matter stress-energy tensor, which we assume to have the *perfect fluid* form:

$$T_{\mu\nu} = (e + p)u_\mu u_\nu + p g_{\mu\nu}, \tag{2}$$

where e denotes the fluid proper energy density, p the fluid pressure, u_μ the fluid 4-velocity, and $g_{\mu\nu}$ the spacetime metric. The third assumption concerns the rotation state of the binary system. Although the realistic rotation state will be an irrotational one (cf. Sec. I), we consider both cases of *synchronized* and *irrotational* states in order to exhibit their differences. The fourth assumption is on the equation of state. For simplicity, we use a *polytropic* one,

$$p = \kappa n^\gamma, \tag{3}$$

where n is the fluid baryon number density and κ and γ are some constants. Here we assume that the two neutron stars have the same equation of state, i.e., the constants κ and γ are identical for both stars. The fifth and last assumption is the IWM one, namely a *conformally flat spatial metric*. Then the full spacetime metric takes the form:

$$ds^2 = -(N^2 - B_i B^i)dt^2 - 2B_i dt dx^i + A^2 f_{ij} dx^i dx^j, \tag{4}$$

N being the lapse function, B^i the shift vector, A the conformal factor, and f_{ij} the flat spatial metric. Under these assumptions, the equations for fluid motion and gravitational field are presented in Paper I.

Relative error in the virial theorem
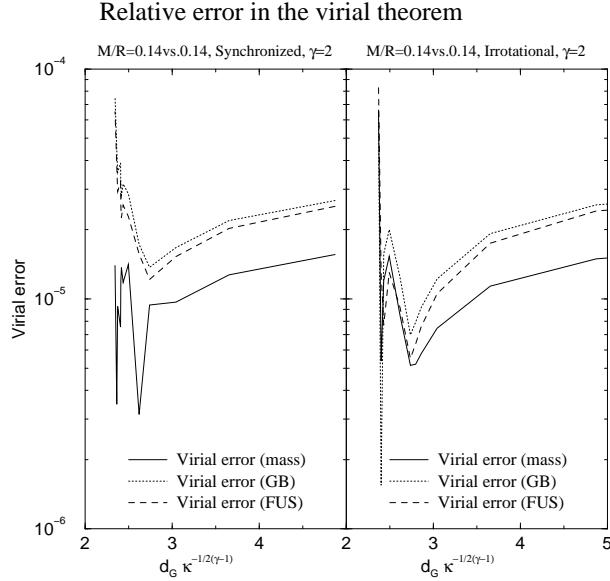
FIG. 1: Relative error in the virial theorem for numerical solutions of relativistic quasiequilibrium binary system, as a function of the orbital separation. Solid, dashed, and dotted lines denote the relative errors defined by Eq. (10), (11) and (12), respectively. Left panel is for synchronized binaries, and the right one for irrotational ones. Both of them are drawn for identical mass binary systems with the compactness $M/R = 0.14$ vs. 0.14.

III.   CODE TESTS

In this series of studies [11, 12, 13, 14], we use a multidomain spectral method with surface-fitted coordinates [42, 43, 44]. This method is implemented by a numerical code constructed upon the C++ library LORENE [45]. Numerous tests of the code have been already presented in Papers I and II. In particular, the comparison with results from other groups [26, 29] has been given in Sec. V.D of Paper I for the identical mass case. We will give here new tests based on the relative error in a general relativistic generalization of the virial theorem.

In Newtonian gravity, the virial theorem has proved to be useful to check the global error in numerical solutions for stationary fluid systems. A general relativistic version of the virial theorem has been obtained by Gourgoulhon and Bonazzola [46] for stationary spacetimes. It has been recently extended to binary star spacetimes within the IWM approximation by Friedman, Uryu and Shibata [41] [2]. The virial relation is equivalent to

$$M_{\text{ADM}} - M_{\text{Komar}} = 0, \tag{5}$$

where M_{ADM} is the ADM mass:

$$M_{\text{ADM}} = -\frac{1}{2\pi} \oint_{\infty} \overline{\nabla}^i A^{1/2} dS_i, \tag{6}$$

and M_{Komar} is a Komar-type mass, defined by

$$M_{\text{Komar}} = \frac{1}{4\pi} \oint_{\infty} \overline{\nabla}^i N dS_i. \tag{7}$$

The virial theorem obtained by Friedman, Uryu and Shibata [41] (see also Eq. (5.7) of Ref. [47]) writes

$$
\begin{aligned}
VE(FUS) &= \int \left[2NA^3 S + \frac{3}{8\pi} NA^3 K_i^j K_j^i + \frac{1}{4\pi} NA(\overline{\nabla}_i \beta \overline{\nabla}^i \beta - \overline{\nabla}_i \nu \overline{\nabla}^i \nu) \right] \\
&= 0.
\end{aligned}
\tag{8}
$$

---

[2] The spacetime generated by a binary system is not stationary, due to gravitational radiation. However, within the IWM approximation, the gravitational radiation is neglected in the global spacetime dynamics, so that one is able to recover the virial theorem.

By a straightforward manipulation, this integral can be recast in the form of the virial theorem as obtained by Gourgoulhon and Bonazzola [46]:

$$VE(GB) = \int \left[2A^3 S + \frac{3}{8\pi} A^3 K_i^j K_j^i + \frac{1}{4\pi} A(\overline{\nabla}_i \beta \overline{\nabla}^i \beta - \overline{\nabla}_i \nu \overline{\nabla}^i \nu - 2\overline{\nabla}_i \beta \overline{\nabla}^i \nu) \right]$$
$$= 0.$$
(9)

Let us stress that the above identity has been derived by Gourgoulhon and Bonazzola [46] only for stationary space-times and that its validity for IWM spacetimes with helical Killing vector has been obtained by Friedman, Uryu and Shibata [41].

As error indicators of our numerical solutions, we have evaluated the quantities

$$\left| \frac{M_{\mathrm{ADM}} - M_{\mathrm{Komar}}}{M_{\mathrm{ADM}}} \right|,$$
(10)

$$\left| \frac{VE(FUS)}{M_{\mathrm{ADM}}} \right|,$$
(11)

$$\left| \frac{VE(GB)}{M_{\mathrm{ADM}}} \right|.$$
(12)

The results are presented in Fig. 1 as a function of the orbital separation. One can see from this figure that the typical virial error is $\sim 1 \times 10^{-5}$ through the sequence.
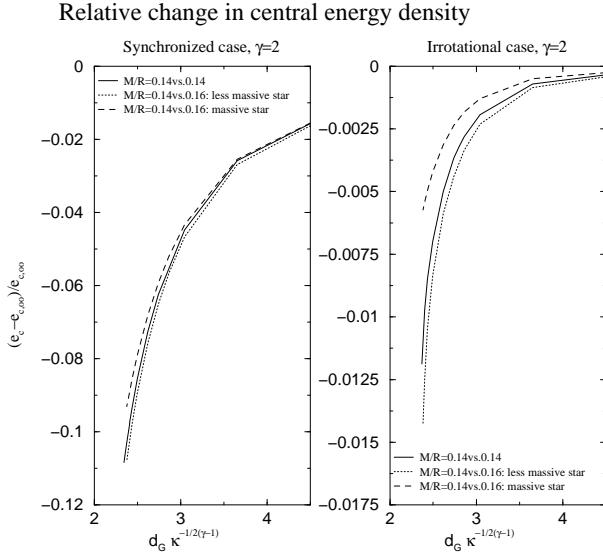

FIG. 2: Relative change in central energy density as a function of the orbital separation between the centers of mass of each star. Left (resp. right) panel is for synchronized (resp. irrotational) binaries with an adiabatic index $\gamma = 2$. Solid line denotes the identical mass case $M/R = 0.14$ vs. 0.14. The results of the different mass case $M/R = 0.14$ vs. 0.16 are shown as dotted (less massive star) and dashed (massive star) lines.

IV. NUMERICAL RESULTS

In this section, we present the numerical results for quasiequilibrium sequences of constant baryon number binaries (evolutionary sequences), for both synchronized and irrotational cases and for the adiabatic index $\gamma = 2$. Although the interesting case is the irrotational one, as mentioned in Sec. I, we have computed configurations for both rotation states in order to compare their properties. The number of computational domains is 4 or 5 for each star and the

space around it. The domains have an onion-like structure, being centered on each star: the innermost domain covers the star, two or three domains (shells) are placed outside it, and the external domain extends to infinity thanks to some compactification (cf. Sec. IV.A of Paper I for all details). The total number of domains is therefore $2 \times 4 = 8$ or $2 \times 5 = 10$. We use 8 domains for close orbital separation and 10 domains for large orbital separation. The numbers of collocation points in each domains are $N_r \times N_\theta \times N_\varphi = 33 \times 25 \times 24$ or $25 \times 17 \times 16$, where N_r, N_θ, and N_φ denote the number of collocation points of the radial, the polar, and the azimuthal directions, respectively.

We parametrize the different mass systems by the values of $(M/R)_{\infty, \text{ star } 1}$ vs. $(M/R)_{\infty, \text{ star } 2}$, where $(M/R)_\infty$ denotes the compactness of the isolated spherical star with the same baryon number.

First of all, the relative changes in central energy density for the cases of $M/R = 0.14$ vs. 0.14 and 0.14 vs. 0.16 are depicted in Fig. 2 as a function of the orbital separation. (Hereafter we abbreviate $(M/R)_{\infty, \text{ star } 1}$ vs. $(M/R)_{\infty, \text{ star } 2}$ as M/R for simplicity.) One can see from these figures that the central energy density decreases monotonically in both synchronized and irrotational cases [3]. The decrease of the central energy density for the synchronized case is about 10 % or more at the end of the sequence, while for the irrotational case, it is only about 1 %.
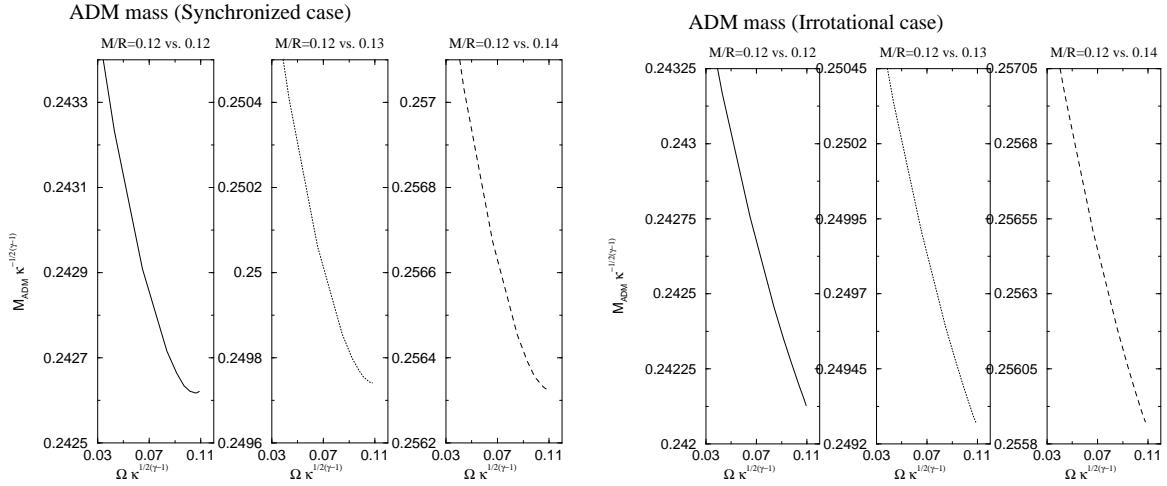
FIG. 3: ADM mass of the binary system as a function of the orbital angular velocity. Left (resp. right) panel is for synchronized (resp. irrotational) binaries. In each panel, the three sub-panels correspond to the compactness of $M/R = 0.12$ vs. 0.12, 0.12 vs. 0.13, and 0.12 vs. 0.14 from the left to the right.

---
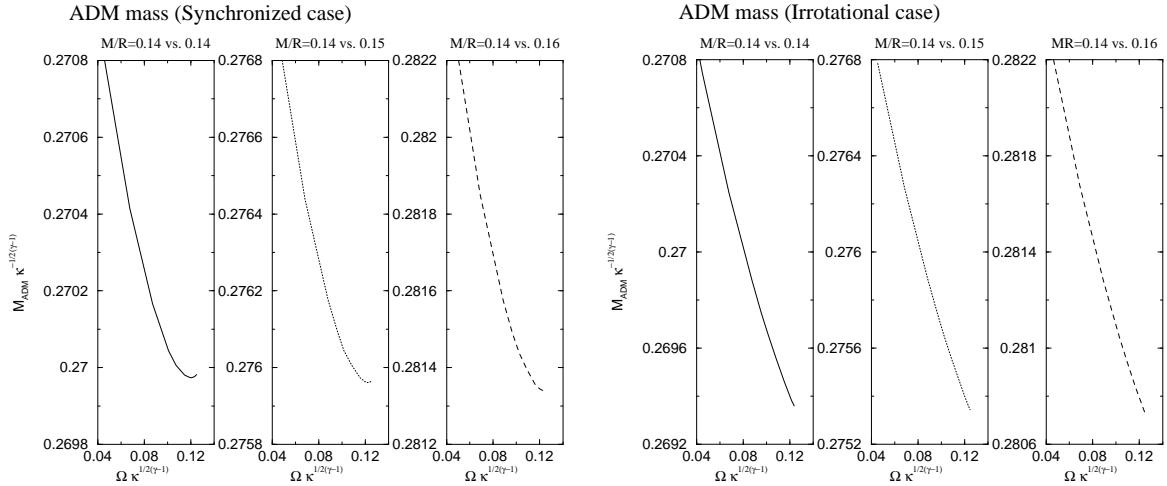
[3] In Paper I (Table III), as well as in [11] (Fig. 1), there was a slight increase in the central energy density for irrotational binaries at the large and medium separations. However, from Paper II we have improved the method to determine the surface of the star, which leads to a better accuracy in the present work.

FIG. 4: Same as Fig. 3, but for the compactness of $M/R = 0.14$ vs. 0.14, 0.14 vs. 0.15, and 0.14 vs. 0.16 from the left to the right in each panel.
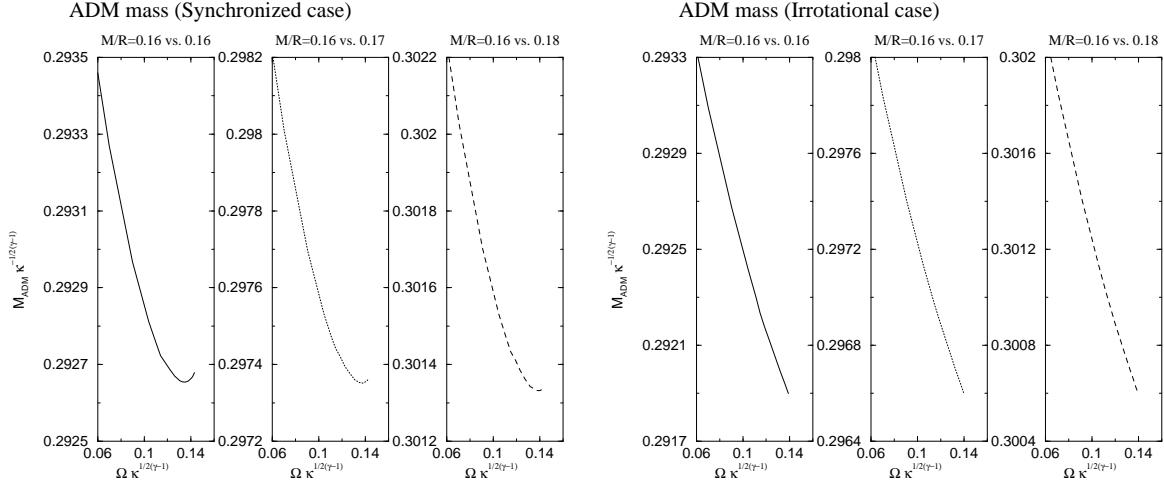
FIG. 5: Same as Fig. 3, but for the compactness of $M/R = 0.16$ vs. 0.16, 0.16 vs. 0.17, and 0.16 vs. 0.18 from the left to the right in each panel.

Next, the ADM mass of the binary system [Eq. (6)] is shown in Figs. $3-5$ as a function of the orbital angular velocity, for different mass ratios and different states of rotation. One can clearly see the turning point in the synchronized cases for identical mass binaries. For more compact stars the turning points appear relatively earlier than those of less compact ones. On the other hand, we do not find any turning point in irrotational binaries. Moreover, it becomes more difficult for the turning point to appear even in the synchronized case when the mass difference in the binary system increases.

In Fig. 6, we show the total angular momentum of the binary system as a function of the orbital angular velocity for the compactness $M/R = 0.18$ vs. 0.18. For synchronized binaries, the turning point of the total angular momentum coincides with that of the ADM mass within the numerical accuracy.
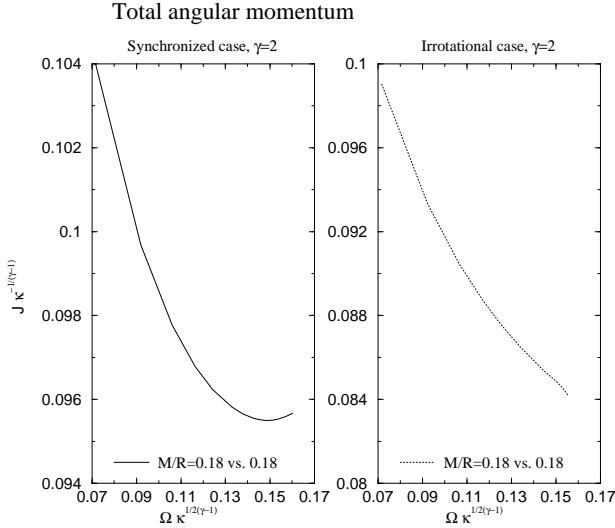
FIG. 6: Total angular momentum of the binary system as a function of the orbital angular velocity for the compactness $M/R = 0.18$ vs. 0.18. Left panel is for the synchronized case and right for the irrotational one.

Equatorial to polar ratio of the radial derivative of enthalpy

Synchronized case, γ=2   Irrotational case, γ=2
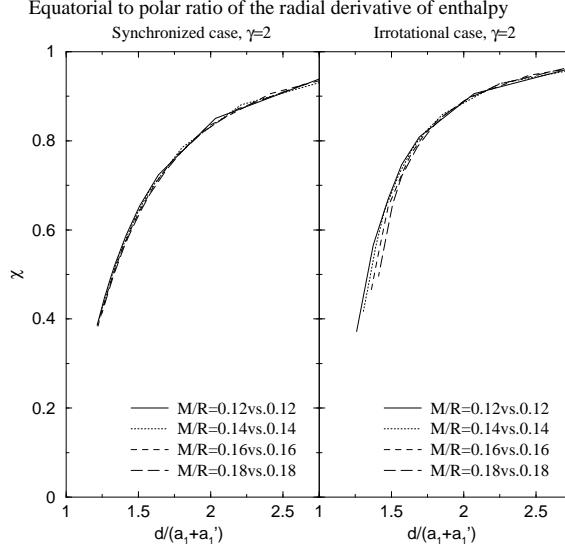
FIG. 7: Equatorial to polar ratio of the radial derivative of the enthalpy as a function of the orbital separation. Left (resp. right) panel is for synchronized (resp. irrotational) binaries. Solid, dotted, dashed, and long-dashed lines denote the cases of the compactness $M/R = 0.12$ vs. 0.12, 0.14 vs. 0.14, 0.16 vs. 0.16, and 0.18 vs. 0.18, respectively.

Equatorial to polar ratio of the radial derivative of enthalpy

Synchronized case, γ=2   Irrotational case, γ=2
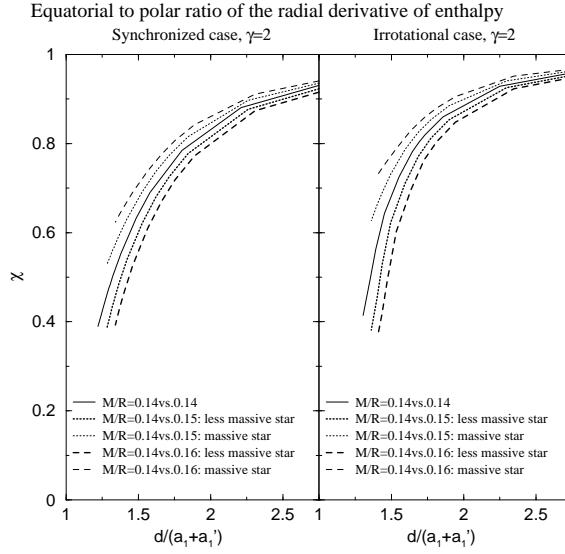
FIG. 8: Same as Fig. 7, but for different mass binaries. Left (resp. right) panel is for synchronized (resp. irrotational) binaries. Solid line denotes the case of identical mass binary with the compactness $M/R = 0.14$. Thin and thick dotted lines are for the compactness $M/R = 0.14$ vs. 0.15 of the more massive and less massive stars, respectively. Thin and thick dashed lines are for the compactness $M/R = 0.14$ vs. 0.16 of the more massive and less massive stars, respectively.

The equatorial to polar ratios of the radial derivative of the enthalpy are shown as a function of the orbital separation normalized by the radius of a star to the companion star in Figs. 7 and 8. As explained in Papers I and II, this quantity

$$\chi := \frac{(\partial H/\partial r)_{\mathrm{eq,comp}}}{(\partial H/\partial r)_{\mathrm{pole}}} \tag{13}$$

is a good dimensionless indicator to detect the appearance of cusp at the stellar surface, which corresponds to the

mass shedding limit. It is worth to plot the variation of χ with respect to the orbital separation normalized by the sum of the radius of each star toward its companion: $d/(a_1 + a_1')$, where d denotes the orbital separation between the two coordinate center (maximum of density), a_1 the radius of the less massive star in the direction of its companion, and a_1' that of the more massive star. Note here that the separation d and the radii a_1 and a_1' are coordinate lengths. If the quantity χ becomes zero, we can conclude that the sequence ends by mass shedding. On the other hand, if the quantity $d/(a_1 + a_1')$ becomes unity, the two stars will contact each other. It is found from Fig. 7 that for synchronized identical mass binaries the sequences seem to terminate by the contact between the two stars (the quantity χ will become zero at the same time). The important feature of the sequences is that they take almost the same track regardless of the compactness. On the contrary, one can see from Fig. 7 that for irrotational binaries the sequences seem to terminate by a cusp point (mass shedding). Such a behavior is enhanced for more compact cases. In Fig. 8, we compare the quantity χ of identical mass binary of the compactness $M/R = 0.14$ with that of different mass binaries of the compactness $M/R = 0.14$ vs. 0.15 and 0.14 vs. 0.16. It is found that the sequences seem to terminate by a cusp point of the less massive star for both synchronized and irrotational binaries when we extrapolate the lines, while the more massive star keeps its shape near spherical one (see the next paragraph). When we increase the difference in mass between two stars, this tendency is enhanced.

It is worth to mention that as soon as the two masses differ, even slightly, the sequence of a synchronized binary system terminates by a cusp point, because the line for the less massive star is always located below that for the identical mass stars which will reach $\chi = 0$ at $d/(a_1 + a_1') = 1$. This implies that the line for the less massive star seems to always reach $\chi = 0$ at $d/(a_1 + a_1') > 1$. Note here that the sequences for identical mass binaries and less massive stars in different mass binaries should reach the point $\chi = 0$. However, in our numerical method, we cannot treat a cuspy figure, because we adapt the innermost numerical domain to the surface of the star and the multidomain spectral method that we use assume that the domain boundaries are smooth surfaces. For very close configurations, it becomes therefore difficult to make the iterative procedure converge to a sufficient level, i.e. to have the relative difference δH in the enthalpy field between two steps lower than 10^{-5}. This explains why we stop the sequences at $\chi \simeq 0.4$. We use $\delta H = 10^{-10}$ for very large separations, $\delta H = 10^{-8} - 10^{-7}$ for medium ones, and $\delta H = 10^{-6} - 10^{-5}$ for very close ones.
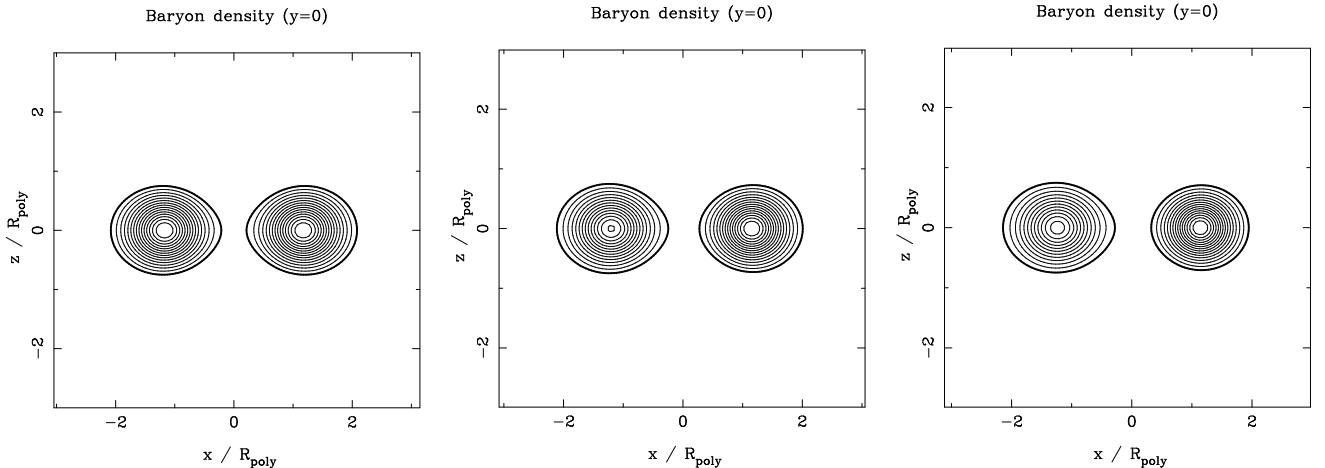
FIG. 9: Isocontours of the baryon density for synchronized binary systems. Left panel is for the compactness $M/R = 0.14$ vs. 0.14, the center panel $M/R = 0.14$ vs. 0.15, and the right panel $M/R = 0.14$ vs. 0.16. The orbital axis is located on $x = 0$ in each panel.

In Figs. 9 and 10, isocontours of the baryon density of various binary systems are shown. There are three panels in each figure. The left panel shows the result for identical mass binary with the compactness $M/R = 0.14$ vs. 0.14. The center and right ones show the results for different mass binaries with the compactness $M/R = 0.14$ vs. 0.15, and 0.14 vs. 0.16, respectively. In these panels, the left hand side star is the less massive star. It is clearly seen that the less massive star is tidally deformed and elongated while the more massive star relatively does not deviate from the spherical shape so much (see the right panel). The orbital separations of these isocontours are listed at the last line of each case in Tables below which corresponds to the closest figure we can calculate, except for the case of $M/R = 0.14$ vs. 0.15 which we do not show in the present paper as a table.

Finally, our numerical results for constant baryon number sequences are presented in Tables I – IV. We represent
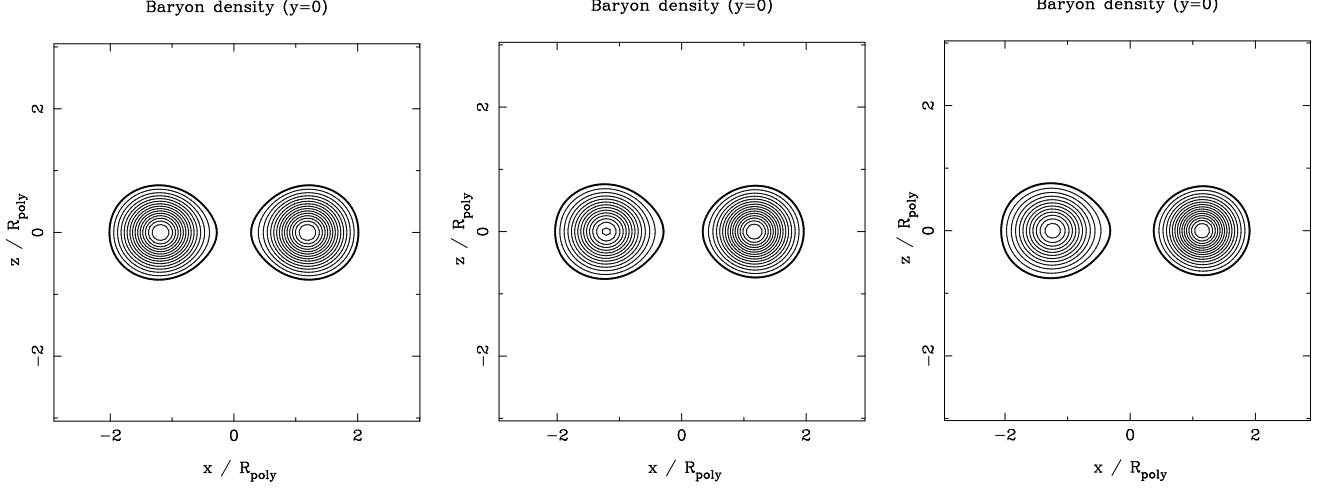
FIG. 10: Same as Fig. 9, but for irrotational binary systems.

the orbital separation by two quantities:

$$\bar{d}_G = \frac{d_G}{R_{\mathrm{poly}}}, \tag{14}$$

$$\bar{d} = \frac{d}{R_{\mathrm{poly}}} . \tag{15}$$

d_G is the coordinate separation between the centers of mass of each star (same definition as Eq. (107) of [29] or Eq. (128) of Paper I), d that between the two stellar centers defined as the maxima of the density field, and R_{poly} the length constructed from the polytropic constants κ and γ [Eq. (3)]

$$R_{\mathrm{poly}} := \kappa^{1/2(\gamma-1)}. \tag{16}$$

The dimensionless orbital angular velocity is defined by

$$\bar{\Omega} := \Omega \kappa^{1/2(\gamma-1)}, \tag{17}$$

the dimensionless ADM mass by

$$\bar{M} := M_{\mathrm{ADM}} \kappa^{-1/2(\gamma-1)}, \tag{18}$$

the dimensionless baryon mass by

$$\bar{M}_{\mathrm{B}} := M_{\mathrm{B}} \kappa^{-1/2(\gamma-1)}, \tag{19}$$

and the dimensionless total angular momentum by

$$\bar{J} := J \kappa^{-1/(\gamma-1)}. \tag{20}$$

The virial errors $VE(\bar{M})$, $VE(\bar{GB})$ and $VE(\bar{FUS})$ are defined by Eqs. (10), (12) and (11) respectively. a_1 denotes the coordinate radius toward the companion star, a_2 the radius perpendicular to it in the orbital plane and a_3 the radius perpendicular to the orbital plane. δe_c is the relative change in central energy density: $\delta e_c := (e_c - e_{c,\infty})/e_{c,\infty}$, and the cusp indicator χ is defined by Eq. (13). In the Tables, the superscript " ' " denotes the values for the more massive star. and the symbol † denotes the turning point in the ADM mass along the sequence.

V. DISCUSSION

In this section, we discuss about the behaviors of the axial ratios, the relative change in central energy density, and the turning point of the synchronized sequences.
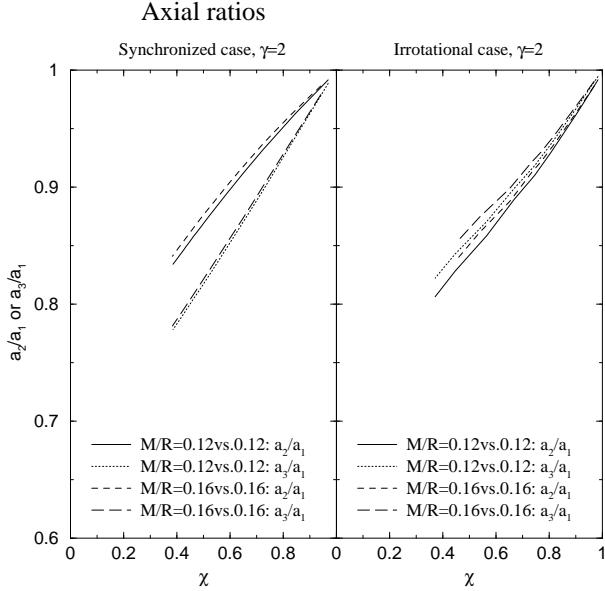
FIG. 11: Axial ratios a_2/a_1 or a_3/a_1 as a function of the cusp indicator χ. Left (resp. right) panel is for synchronized (resp. irrotational) binaries. Solid and dotted lines denote the axial ratios a_2/a_1 and a_3/a_1 for the compactness $M/R = 0.12$ vs. 0.12, respectively. Dashed and long-dashed lines are the axial ratios a_2/a_1 and a_3/a_1 for the compactness $M/R = 0.16$ vs. 0.16, respectively.

In Figs. 11 and 12, the axial ratios are shown as a function of the cusp indicator χ. In Fig. 11, we show the axial ratios a_2/a_1 and a_3/a_1 for identical mass binaries with the compactness $M/R = 0.12$ vs. 0.12 and 0.16 vs. 0.16. One can see from this figure that each axial ratio has almost the same track regardless of the difference of the compactness, in particular for synchronized binary systems. Moreover, such a coincidence of the sequence appears in the cases of different mass binary systems (see Fig. 12). In those cases, the sequences almost coincide with each other regardless of the compactness of the companion star. Note that the sequences of the axial ratios for more massive stars end before $\chi = 0$, while those for less massive stars should reach the point $\chi = 0$. However we cannot treat a cuspy figure with our numerical method, because we adapt the innermost numerical domain to the surface of the star and the domain boundaries are assumed to be smooth (see discussion in Sec. IV). Therefore we had to stop the sequences at around $\chi = 0.4$ for the less massive star.

The relative change in central energy density is presented as a function of χ in Fig. 13. It is clearly seen that the sequences for the synchronized case with the same compactness coincide with each other, while those with the different compactness split into curves with respect to each compactness. For example, the relative change for the identical binary system with the compactness $M/R = 0.14$ coincides with that for the more massive star of the different mass binary with $M/R = 0.12$ vs. 0.14 and that for the less massive star with $M/R = 0.14$ vs. 0.16. However, the sequences for stars with $M/R = 0.12$, 0.14, and 0.16 are different from each other.

Finally, let us comment on the behavior of the turning point of the ADM mass (binding energy) along a sequence. We never found any turning points for irrotational binary systems with the polytropic index $\gamma = 2$. On the other hand, it appeared clearly for the synchronized case. In Fig. 14, the cusp indicator χ at the turning point of synchronized identical mass binary systems is plotted as a function of the compactness M/R. Since the accuracy of the determination of the ADM mass is order of 10^{-5} in our calculations, the relative errors on the orbital angular velocity and the quantity χ at the turning point become a few percents. Even when one is taking this fact into account, it is possible to conclude that the line in Fig. 14 increases proportionally to the compactness of the stars. This behavior agrees with the value of χ_{turning} that we have found in Newtonian calculations ($M/R = 0$), namely $\chi_{\text{turning}} = 0.2862$ (Table I of Paper II).

VI. SUMMARY

In the present paper, we have computed constant baryon number sequences of binary neutron stars in quasiequilibrium, in both cases of synchronized and irrotational motion and in both cases of identical and different mass systems. We have performed a general relativistic treatment, within the IWM approximation (conformally flat spatial metric).
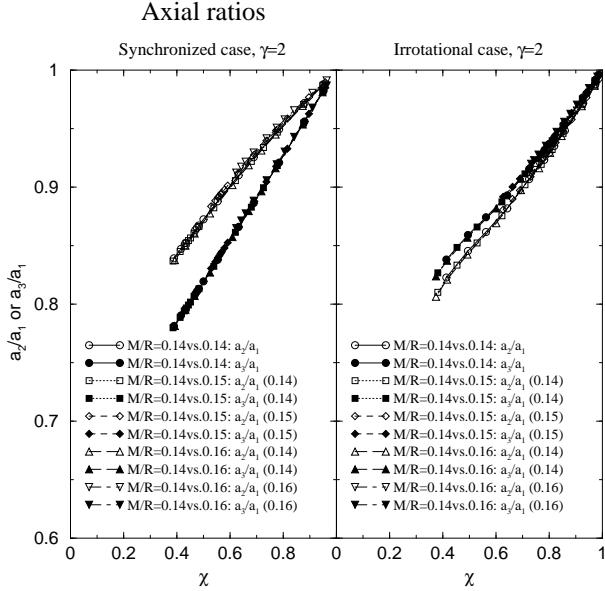
FIG. 12: Same as Fig. 11 but for different mass binaries. Solid line with open and filled circles denote the axial ratios a_2/a_1 and a_3/a_1 of the compactness $M/R = 0.14$ vs. 0.14, respectively. Dotted line with open and filled squares denote the axial ratios a_2/a_1 and a_3/a_1 of the compactness $M/R = 0.14$ vs. 0.15 for less massive star, respectively. Dashed line with open and filled diamonds denote the axial ratios a_2/a_1 and a_3/a_1 of the compactness $M/R = 0.14$ vs. 0.15 for more massive star, respectively. Long-dashed line with open and filled triangle-up denote the axial ratios a_2/a_1 and a_3/a_1 of the compactness $M/R = 0.14$ vs. 0.16 for less massive star, respectively. Dot-dashed line with open and filled triangle-down denote the axial ratios a_2/a_1 and a_3/a_1 of the compactness $M/R = 0.14$ vs. 0.16 for more massive star, respectively.

We have used a polytropic equation of state with an adiabatic index $\gamma = 2$.

The summary of our results is that (1) Among the quasiequilibrium sequences we have calculated in the present article, only the synchronized identical star binaries terminate by the contact between two stars, while all the other types of sequences (synchronized different star binaries, irrotational identical star and different star binaries) end at the mass shedding points. Note here that we cannot conclude about the end points of *non-quasiequilibrium* sequences (i.e. dynamical sequences), such that binary systems without viscosity but with intrinsic non-aligned spins, those with slight viscosity and deviating from both the irrotational state and the synchronized one, those with infalling radial velocity, and so on. (2) For identical mass binary systems there is no turning point of the ADM mass in the irrotational case, while there is clearly one before the end point of the sequence in the synchronized case. (3) It is more difficult to see the turning points of the ADM mass for different mass binary systems than for identical ones. (4) The deformation of the star is determined by the orbital separation and the mass ratio and is not affected much by its compactness. (5) The decrease of the central energy density depends on the compactness of the star and not on that of its companion.

Acknowledgments

[1] H. Tagoshi et al, Phys. Rev. D **63**, 062001 (2001).

Relative change in central energy density
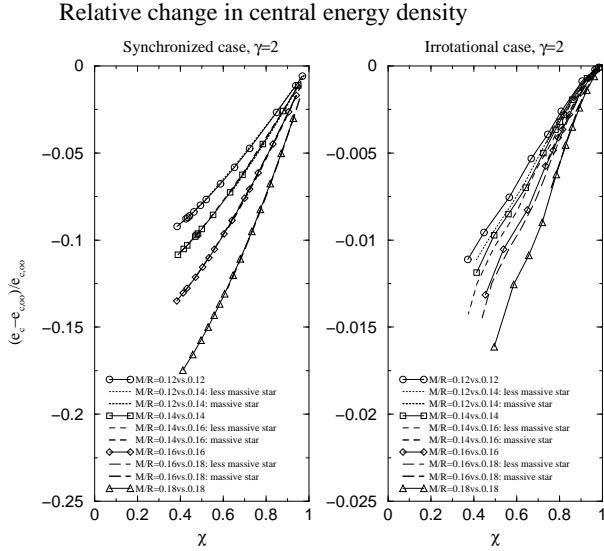
FIG. 13: Relative change in central energy density as a function of the cusp indicator χ. Left (resp. right) panel is for synchronized (resp. irrotational) binaries. Solid lines with open circle, square, diamond, and triangle denote the cases of the identical mass binaries with the compactness $M/R = 0.12$ vs. 0.12, 0.14 vs. 0.14, 0.16 vs. 0.16, and 0.18 vs. 0.18, respectively. Thin and thick dotted lines are for the compactness $M/R = 0.12$ vs. 0.14 of the less massive and more massive stars, respectively. Thin and thick dashed lines are for the compactness $M/R = 0.14$ vs. 0.16 of the less massive and more massive stars, respectively. Thin and thick long-dashed lines are for the compactness $M/R = 0.16$ vs. 0.18 of the less massive and more massive stars, respectively.
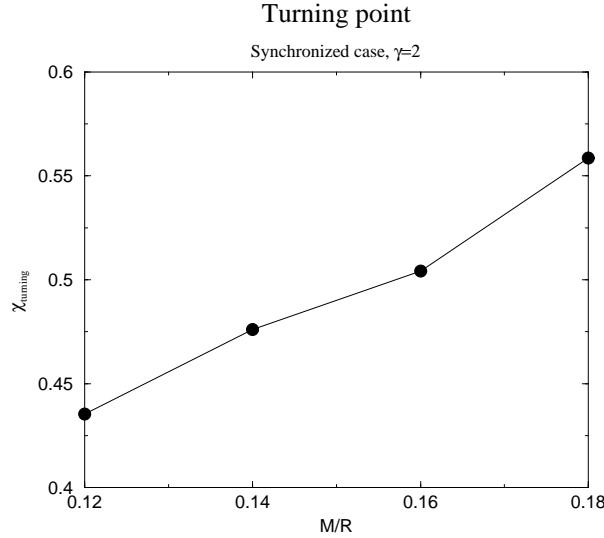
Turning point

FIG. 14: Cusp indicator χ at the turning point of the ADM mass along a sequence of synchronized identical mass binaries, as a function of the compactness M/R.

[2] R. Narayan, B. Paczynski, and T. Piran, Astrophys. J. Lett. **395**, L83 (1992).
[3] P. Jaranowski and G. Schäfer, Phys. Rev. D **57**, 7274 (1998); *ibid.* **60**, 124003 (1999). T. Damour, P. Jaranowski, and G. Schäfer, Phys. Rev. D **62**, 044024 (2000).
[4] L. Blanchet and G. Faye, Phys. Lett. **A271**, 58 (2000); Phys. Rev. D **63**, 062005 (2001).
[5] T. Damour, P. Jaranowski, and G. Schäfer, Phys. Rev. D **63**, 044021 (2001).
[6] V. de Andrade, L. Blanchet, and G. Faye, Class. Quant. Grav. **18**, 753 (2001).

 [7] M. Shibata, Phys. Rev. D **60**, 104052 (1999).
 [8] M. Shibata and K. Uryu, Phys. Rev. D **61**, 064001 (2000).
 [9] K. Oohara and T. Nakamura, Prog. Theor. Phys. Suppl. **136**, 270 (1999).
[10] J.A. Font, T. Goodale, S. Iyer, M. Miller, L. Rezzolla, E. Seidel, N. Stergioulas, W.-M. Suen, and M. Tobias, Phys. Rev. D **65**, 084024 (2002).
[11] S. Bonazzola, E. Gourgoulhon, and J.-A. Marck, Phys. Rev. Lett. **82**, 892 (1999).
[12] E. Gourgoulhon, P. Grandclément, K. Taniguchi, J.-A. Marck, and S. Bonazzola, Phys. Rev. D **63**, 064029 (2001): Paper I.
[13] K. Taniguchi, E. Gourgoulhon, and S. Bonazzola, Phys. Rev. D **64**, 064012 (2001): Paper II.
[14] K. Taniguchi and E. Gourgoulhon, Phys. Rev. D **65**, 044027 (2002).
[15] J. A. Faber, P. Grandclément, F. A. Rasio, and K. Taniguchi, submitted to Phys. Rev. Lett., preprint astro-ph/0204397. See also M. Saijo and T. Nakamura, Phys. Rev. Lett. **85**, 2665 (2000), *ibid.* Phys, Rev. D **63**, 064004 (2001), for a different idea to determine the radius of a neutron star.
[16] D. Lai, F. A. Rasio, and S. L. Shapiro, Astrophys. J. Suppl. Ser. **88**, 205 (1993); Astrophys. J. **420**, 811 (1994).
[17] K. Taniguchi and T. Nakamura, Phys. Rev. Lett. **84**, 581 (2000); Phys. Rev. D **62**, 044040 (2000).
[18] J. C. Lombardi, F. A. Rasio, and S. L. Shapiro, Phys. Rev. D **56**, 3416 (1997).
[19] K. Taniguchi and M. Shibata, Phys. Rev. D **56**, 798 (1997).
[20] M. Shibata and K. Taniguchi, Phys. Rev. D **56**, 811 (1997).
[21] K. Taniguchi, Prog. Theor. Phys. **101**, 283 (1999).
[22] I. Hachisu and Y. Eriguchi, Publ. Astron. Soc. Jpn. **36**, 239 (1984).
[23] I. Hachisu and Y. Eriguchi, Publ. Astron. Soc. Jpn. **36**, 259 (1984).
[24] K. Uryu and Y. Eriguchi, Astrophys. J. Suppl. Ser. **118**, 563 (1998).
[25] M. Shibata, Prog. Theor. Phys. **96**, 317 (1996); Phys. Rev. D **55**, 6019 (1997).
[26] T. W. Baumgarte, G. B. Cook, M. A. Scheel, S. L. Shapiro, and S. A. Teukolsky, Phys. Rev. Lett. **79**, 1182 (1997); Phys. Rev. D **57**, 7299 (1998).
[27] P. Marronetti, G.J. Mathews, and J.R. Wilson, Phys. Rev. D **58**, 107503 (1998).
[28] P. Marronetti, G.J. Mathews, and J.R. Wilson, Phys. Rev. D **60**, 087301 (1999).
[29] K. Uryu and Y. Eriguchi, Phys. Rev. D **61**, 124023 (2000).
[30] K. Uryu, M. Shibata, and Y. Eriguchi, Phys. Rev. D **62**, 104015 (2000).
[31] F. Usui, K. Uryu, and Y. Eriguchi, Phys. Rev. D **61**, 024039 (1999).
[32] F. Usui and Y. Eriguchi, Phys. Rev. D **65**, 064030 (2002).
[33] C. S. Kochaneck, Astrophys. J. **398**, 234 (1992).
[34] L. Bildsten and C. Cutler, Astrophys. J. **400**, 175 (1992).
[35] S. Bonazzola, E. Gourgoulhon, and J.-A. Marck, Phys. Rev. D **56**, 7740 (1997).
[36] H. Asada, Phys. Rev. D **57**, 7292 (1998).
[37] M. Shibata, Phys. Rev. D **58**, 024012 (1998).
[38] S. A. Teukolsky, Astrophys. J. **504**, 442 (1998).
[39] J. Isenberg and J. Nester, in *General Relativity and Gravitation*, edited by A. Held (Plenum, New York, 1980), Vol. 1.
[40] J.R. Wilson and G.J. Mathews, in *Frontiers in numerical relativity*, edited by C.R. Evans, L.S. Finn and D.W. Hobill (Cambridge University Press, Cambridge, England, 1989).
[41] J. L. Friedman, K. Uryu, and M. Shibata, Phys. Rev. D **65**, 064035 (2002).
[42] S. Bonazzola, E. Gourgoulhon, and J.-A. Marck, Phys. Rev. D **58**, 104020 (1998).
[43] S. Bonazzola, E. Gourgoulhon, and J.-A. Marck, J. Comput. Appl. Math. **109**, 433 (1999).
[44] P. Grandclément, S. Bonazzola, E. Gourgoulhon and J.-A. Marck, J. Comput. Phys. **170**, 231 (2001).
[45] `http://www.lorene.obspm.fr/`
[46] E. Gourgoulhon and S. Bonazzola, Class. Quantum Grav. **11**, 443 (1994).
[47] M. Shibata and K. Uryu, Phys. Rev. D **64**, 104017 (2001).

TABLE I: Orbital angular velocity, ADM mass, total angular momentum, virial errors, axial ratios, relative change in central energy density, and the cusp indicator χ along constant baryon number sequences of identical mass binaries in synchronized motion, for various compactness. The symbol † denotes the turning point of the sequences.

$\bar{d}_G$	$\tilde{d}$	$\bar{\Omega}$	$\bar{M}$	$\bar{J}$	$|V\bar{E}(M)|$	$|V\bar{E}(GB)|$	$|V\bar{E}(FUS)|$	a_2/a_1	a_3/a_1	δe_c	χ
						Identical mass stars, Synchronized case					
				$M/R = 0.12$ vs. 0.12,		$\bar{M}_B = 0.1299$ vs. 0.1299					
4.873	2.757	4.299(-2)	0.2432	7.675(-2)	8.840(-6)	1.453(-5)	1.350(-5)	0.9846	0.9773	-1.136(-2)	0.9395
3.655	2.033	6.473(-2)	0.2429	7.057(-2)	6.931(-6)	1.142(-5)	1.042(-5)	0.9637	0.9438	-2.675(-2)	0.8500
3.046	1.639	8.366(-2)	0.2427	6.793(-2)	6.181(-6)	8.837(-6)	7.788(-6)	0.9317	0.8970	-4.736(-2)	0.7236
2.864	1.509	9.125(-2)	0.2427	6.733(-2)	4.256(-6)	7.069(-6)	6.307(-6)	0.9126	0.8713	-5.820(-2)	0.6531
2.742	1.415	9.701(-2)	0.2426	6.703(-2)	5.475(-6)	6.589(-6)	5.809(-6)	0.8942	0.8478	-6.772(-2)	0.5875
2.650	1.338	1.018(-1)	0.2426	6.688(-2)	8.194(-7)	8.531(-6)	7.661(-6)	0.8752	0.8246	-7.666(-2)	0.5214
† 2.565	1.255	1.066(-1)	0.2426	6.684(-2)	8.662(-6)	2.064(-5)	1.707(-5)	0.8492	0.7949	-8.698(-2)	0.4353
2.559	1.249	1.070(-1)	0.2426	6.684(-2)	4.567(-6)	2.755(-5)	2.337(-5)	0.8470	0.7924	-8.781(-2)	0.4278
2.528	1.215	1.089(-1)	0.2426	6.685(-2)	1.195(-6)	3.725(-5)	3.236(-5)	0.8342	0.7783	-9.223(-2)	0.3858
				$M/R = 0.14$ vs. 0.14,		$\bar{M}_B = 0.1461$ vs. 0.1461					
4.873	2.979	4.505(-2)	0.2708	9.090(-2)	1.558(-5)	2.677(-5)	2.525(-5)	0.9877	0.9821	-1.119(-2)	0.9513
3.655	2.211	6.764(-2)	0.2704	8.357(-2)	1.271(-5)	2.189(-5)	2.026(-5)	0.9720	0.9560	-2.588(-2)	0.8805
3.046	1.803	8.719(-2)	0.2702	8.031(-2)	9.695(-6)	1.673(-5)	1.527(-5)	0.9494	0.9209	-4.480(-2)	0.7846
2.742	1.581	1.008(-1)	0.2700	7.902(-2)	9.415(-6)	1.372(-5)	1.214(-5)	0.9253	0.8864	-6.247(-2)	0.6900
2.620	1.485	1.074(-1)	0.2700	7.864(-2)	3.142(-6)	1.728(-5)	1.568(-5)	0.9099	0.8658	-7.263(-2)	0.6326
2.499	1.380	1.147(-1)	0.2700	7.839(-2)	1.412(-5)	2.865(-5)	2.280(-5)	0.8878	0.8378	-8.559(-2)	0.5538
† 2.413	1.297	1.203(-1)	0.2700	7.833(-2)	1.192(-5)	3.127(-5)	2.535(-5)	0.8652	0.8108	-9.715(-2)	0.4761
2.377	1.258	1.229(-1)	0.2700	7.834(-2)	9.280(-6)	3.548(-5)	2.930(-5)	0.8522	0.7960	-1.030(-1)	0.4328
2.346	1.221	1.252(-1)	0.2700	7.836(-2)	1.396(-5)	7.557(-5)	6.519(-5)	0.8390	0.7814	-1.084(-1)	0.3893
				$M/R = 0.16$ vs. 0.16,		$\bar{M}_B = 0.1600$ vs. 0.1600					
4.264	2.829	5.634(-2)	0.2935	9.912(-2)	2.509(-5)	4.471(-5)	4.242(-5)	0.9862	0.9791	-1.699(-2)	0.9417
3.655	2.414	6.990(-2)	0.2933	9.497(-2)	2.255(-5)	4.021(-5)	3.777(-5)	0.9786	0.9662	-2.641(-2)	0.9059
3.046	1.983	8.992(-2)	0.2930	9.114(-2)	1.815(-5)	3.248(-5)	3.011(-5)	0.9626	0.9397	-4.486(-2)	0.8328
2.620	1.659	1.104(-1)	0.2928	8.898(-2)	1.382(-5)	2.393(-5)	2.181(-5)	0.9367	0.9005	-7.066(-2)	0.7240
2.438	1.506	1.218(-1)	0.2927	8.836(-2)	2.887(-5)	4.340(-5)	3.510(-5)	0.9153	0.8708	-8.872(-2)	0.6414
2.316	1.393	1.306(-1)	0.2927	8.813(-2)	2.270(-5)	3.892(-5)	3.056(-5)	0.8929	0.8419	-1.053(-1)	0.5597
† 2.255	1.331	1.354(-1)	0.2927	8.810(-2)	2.050(-5)	3.994(-5)	3.153(-5)	0.8771	0.8226	-1.156(-1)	0.5042
2.194	1.261	1.405(-1)	0.2927	8.815(-2)	3.159(-6)	6.903(-5)	5.741(-5)	0.8556	0.7975	-1.277(-1)	0.4312
2.164	1.220	1.432(-1)	0.2927	8.821(-2)	3.129(-5)	5.921(-5)	5.015(-5)	0.8409	0.7813	-1.350(-1)	0.3837
				$M/R = 0.18$ vs. 0.18,		$\bar{M}_B = 0.1710$ vs. 0.1710					
3.655	2.650	7.156(-2)	0.3108	1.040(-1)	3.917(-5)	7.192(-5)	6.851(-5)	0.9840	0.9745	-3.007(-2)	0.9273
3.046	2.188	9.193(-2)	0.3104	9.968(-2)	3.292(-5)	6.062(-5)	5.706(-5)	0.9726	0.9547	-5.015(-2)	0.8716
2.559	1.796	1.163(-1)	0.3101	9.679(-2)	2.624(-5)	4.584(-5)	4.207(-5)	0.9512	0.9201	-8.243(-2)	0.7743
2.316	1.581	1.330(-1)	0.3100	9.582(-2)	3.933(-5)	6.381(-5)	5.182(-5)	0.9284	0.8865	-1.108(-1)	0.6802
2.194	1.463	1.428(-1)	0.3100	9.555(-2)	3.324(-5)	3.124(-5)	2.506(-5)	0.9094	0.8607	-1.308(-1)	0.6071
† 2.134	1.398	1.482(-1)	0.3100	9.550(-2)	2.666(-5)	6.812(-5)	5.487(-5)	0.8962	0.8436	-1.431(-1)	0.5585
2.073	1.328	1.540(-1)	0.3100	9.554(-2)	2.113(-5)	7.194(-5)	5.803(-5)	0.8788	0.8220	-1.574(-1)	0.4966
2.042	1.290	1.571(-1)	0.3100	9.559(-2)	1.005(-7)	1.085(-4)	8.977(-5)	0.8675	0.8087	-1.656(-1)	0.4581
2.012	1.248	1.602(-1)	0.3100	9.567(-2)	4.965(-5)	1.943(-4)	1.632(-4)	0.8537	0.7930	-1.747(-1)	0.4120

TABLE II: Same as Table I but for different mass binary systems. The superscript " ' " denotes the values for the more massive star.

$\bar{d}_G$	$\tilde{d}$	$\bar{\Omega}$	$\bar{M}$	$\bar{J}$	$|VE(\bar{M})|$	$|VE(\bar{GB})|$	$|VE(\bar{FUS})|$	a_2/a_1 a'_2/a'_1	a_3/a_1 a'_3/a'_1	δe_c $\delta e'_c$	χ χ'
						Different mass stars, Synchronized case					
					$M/R = 0.12$ vs. 0.14,	$\bar{M}_B = 0.1299$ vs. 0.1461					
4.873	2.863	4.404(-2)	0.2570	8.347(-2)	1.201(-5)	2.022(-5)	1.895(-5)	0.9827	0.9754	-1.197(-2)	0.9345
								0.9891	0.9833	-1.066(-2)	0.9548
3.655	2.117	6.621(-2)	0.2567	7.675(-2)	9.690(-6)	1.633(-5)	1.501(-5)	0.9593	0.9391	-2.824(-2)	0.8376
								0.9750	0.9592	-2.467(-2)	0.8891
3.046	1.715	8.547(-2)	0.2565	7.382(-2)	7.292(-6)	1.220(-5)	1.106(-5)	0.9234	0.8882	-5.023(-2)	0.7001
								0.9547	0.9265	-4.264(-2)	0.8001
2.864	1.583	9.317(-2)	0.2564	7.312(-2)	6.226(-6)	1.043(-5)	9.430(-6)	0.9018	0.8600	-6.189(-2)	0.6227
								0.9434	0.9095	-5.169(-2)	0.7532
2.742	1.488	9.899(-2)	0.2564	7.275(-2)	1.408(-5)	1.812(-5)	1.523(-5)	0.8807	0.8338	-7.209(-2)	0.5501
								0.9330	0.8946	-5.930(-2)	0.7121
2.681	1.437	1.022(-1)	0.2563	7.261(-2)	1.605(-5)	2.080(-5)	1.631(-5)	0.8665	0.8170	-7.840(-2)	0.5026
								0.9265	0.8856	-6.392(-2)	0.6870
2.620	1.383	1.055(-1)	0.2563	7.249(-2)	1.185(-5)	2.514(-5)	2.050(-5)	0.8486	0.7965	-8.565(-2)	0.4439
								0.9190	0.8753	-6.900(-2)	0.6582
2.577	1.342	1.080(-1)	0.2563	7.243(-2)	1.161(-6)	4.051(-5)	3.446(-5)	0.8327	0.7789	-9.144(-2)	0.3923
								0.9128	0.8671	-7.294(-2)	0.6352
					$M/R = 0.14$ vs. 0.16,	$\bar{M}_B = 0.1461$ vs. 0.1600					
4.873	3.102	4.586(-2)	0.2823	9.688(-2)	2.076(-5)	3.649(-5)	3.473(-5)	0.9865	0.9810	-1.164(-2)	0.9484
								0.9912	0.9869	-1.119(-2)	0.9635
3.655	2.307	6.879(-2)	0.2818	8.905(-2)	1.736(-5)	3.055(-5)	2.855(-5)	0.9694	0.9534	-2.691(-2)	0.8733
								0.9805	0.9679	-2.550(-2)	0.9110
3.046	1.888	8.858(-2)	0.2816	8.552(-2)	1.370(-5)	2.420(-5)	2.232(-5)	0.9449	0.9161	-4.664(-2)	0.7717
								0.9657	0.9429	-4.331(-2)	0.8417
2.742	1.662	1.024(-1)	0.2814	8.408(-2)	1.132(-5)	1.941(-5)	1.771(-5)	0.9186	0.8794	-6.518(-2)	0.6711
								0.9507	0.9193	-5.931(-2)	0.7762
2.620	1.564	1.090(-1)	0.2814	8.364(-2)	2.342(-5)	3.453(-5)	2.770(-5)	0.9016	0.8572	-7.584(-2)	0.6096
								0.9416	0.9056	-6.817(-2)	0.7384
2.499	1.460	1.163(-1)	0.2814	8.329(-2)	2.577(-5)	3.575(-5)	2.861(-5)	0.8774	0.8271	-8.945(-2)	0.5251
								0.9295	0.8882	-7.911(-2)	0.6897
2.438	1.403	1.203(-1)	0.2813	8.318(-2)	1.268(-5)	4.801(-5)	3.990(-5)	0.8603	0.8071	-9.800(-2)	0.4677
								0.9217	0.8775	-8.567(-2)	0.6595
2.377	1.341	1.245(-1)	0.2813	8.310(-2)	1.713(-5)	1.014(-4)	8.814(-5)	0.8376	0.7814	-1.079(-1)	0.3927
								0.9124	0.8650	-9.308(-2)	0.6238
					$M/R = 0.16$ vs. 0.18,	$\bar{M}_B = 0.1600$ vs. 0.1710					
4.264	2.957	5.704(-2)	0.3023	1.037(-1)	3.359(-5)	6.089(-5)	5.824(-5)	0.9852	0.9782	-1.745(-2)	0.9393
								0.9901	0.9848	-1.904(-2)	0.9566
3.655	2.526	7.074(-2)	0.3020	9.936(-2)	3.049(-5)	5.543(-5)	5.256(-5)	0.9772	0.9648	-2.712(-2)	0.9021
								0.9850	0.9754	-2.934(-2)	0.9301
3.046	2.080	9.094(-2)	0.3017	9.529(-2)	2.522(-5)	4.605(-5)	4.311(-5)	0.9602	0.9373	-4.608(-2)	0.8260
								0.9743	0.9564	-4.896(-2)	0.8764
2.620	1.747	1.116(-1)	0.3015	9.293(-2)	1.940(-5)	3.529(-5)	3.267(-5)	0.9328	0.8963	-7.264(-2)	0.7127
								0.9577	0.9289	-7.522(-2)	0.7990
2.438	1.592	1.230(-1)	0.3014	9.221(-2)	3.520(-5)	5.539(-5)	4.539(-5)	0.9100	0.8653	-9.132(-2)	0.6266
								0.9448	0.9089	-9.288(-2)	0.7431
2.316	1.479	1.318(-1)	0.3013	9.188(-2)	3.541(-5)	5.009(-5)	4.242(-5)	0.8862	0.8350	-1.085(-1)	0.5411
								0.9324	0.8907	-1.081(-1)	0.6915
2.237	1.398	1.381(-1)	0.3013	9.177(-2)	1.418(-5)	7.574(-5)	6.303(-5)	0.8633	0.8075	-1.226(-1)	0.4625
								0.9214	0.8753	-1.204(-1)	0.6480
2.194	1.350	1.417(-1)	0.3013	9.174(-2)	1.249(-5)	1.266(-4)	1.084(-4)	0.8465	0.7883	-1.315(-1)	0.4063
								0.9141	0.8655	-1.278(-1)	0.6200

TABLE III: Same as Table I, but for irrotational binaries.

$\bar{d}_G$	$\tilde{d}$	$\bar{\Omega}$	$\bar{M}$	$\bar{J}$	$|V\bar{E}(M)|$	$|V\bar{E}(GB)|$	$|V\bar{E}(\bar{F}US)|$	a_2/a_1	a_3/a_1	δe_c	χ
				Identical mass stars, Irrotational case							
				$M/R = 0.12$ vs. 0.12, $\bar{M}_{\rm B} = 0.1299$ vs. 0.1299							
6.090	3.472	3.120(-2)	0.2434	8.076(-2)	9.264(-6)	1.530(-5)	1.439(-5)	0.9916	0.9945	-8.061(-5)	0.9837
4.872	2.780	4.304(-2)	0.2432	7.365(-2)	8.394(-6)	1.371(-5)	1.266(-5)	0.9846	0.9882	-2.038(-4)	0.9654
3.653	2.072	6.488(-2)	0.2428	6.589(-2)	5.992(-6)	9.535(-6)	8.445(-6)	0.9631	0.9681	-8.804(-4)	0.9055
3.044	1.694	8.397(-2)	0.2425	6.180(-2)	3.377(-6)	4.933(-6)	3.962(-6)	0.9299	0.9369	-2.613(-3)	0.8082
2.861	1.570	9.164(-2)	0.2423	6.058(-2)	6.164(-6)	8.369(-6)	6.394(-6)	0.9100	0.9183	-3.929(-3)	0.7459
2.738	1.478	9.746(-2)	0.2423	5.978(-2)	4.595(-6)	6.938(-6)	5.079(-6)	0.8896	0.8988	-5.328(-3)	0.6692
2.616	1.375	1.040(-1)	0.2422	5.900(-2)	1.337(-5)	1.239(-5)	7.816(-6)	0.8582	0.8705	-7.548(-3)	0.5655
2.554	1.304	1.076(-1)	0.2422	5.864(-2)	5.612(-7)	1.134(-6)	6.392(-6)	0.8283	0.8428	-9.566(-3)	0.4476
2.523	1.259	1.095(-1)	0.2421	5.846(-2)	2.005(-5)	5.038(-6)	1.880(-5)	0.8064	0.8223	-1.111(-2)	0.3720
				$M/R = 0.14$ vs. 0.14, $\bar{M}_{\rm B} = 0.1461$ vs. 0.1461							
4.872	3.001	4.510(-2)	0.2707	8.755(-2)	1.494(-5)	2.565(-5)	2.409(-5)	0.9877	0.9914	-1.870(-4)	0.9736
3.653	2.249	6.780(-2)	0.2702	7.858(-2)	1.136(-5)	1.924(-5)	1.748(-5)	0.9717	0.9766	-7.114(-4)	0.9284
3.044	1.856	8.753(-2)	0.2699	7.384(-2)	7.459(-6)	1.222(-5)	1.054(-5)	0.9483	0.9545	-1.940(-3)	0.8594
2.739	1.645	1.014(-1)	0.2697	7.146(-2)	5.141(-6)	6.971(-6)	5.511(-6)	0.9231	0.9309	-3.673(-3)	0.7812
2.617	1.553	1.080(-1)	0.2696	7.053(-2)	8.504(-6)	1.243(-5)	9.189(-6)	0.9067	0.9154	-5.005(-3)	0.7255
2.495	1.453	1.154(-1)	0.2695	6.962(-2)	1.532(-5)	2.005(-5)	1.304(-5)	0.8819	0.8929	-6.999(-3)	0.6432
2.433	1.392	1.195(-1)	0.2694	6.918(-2)	1.200(-5)	1.575(-5)	7.702(-6)	0.8616	0.8742	-8.502(-3)	0.5623
2.403	1.353	1.216(-1)	0.2694	6.896(-2)	5.376(-6)	1.547(-6)	1.295(-5)	0.8453	0.8591	-9.722(-3)	0.4950
2.372	1.305	1.238(-1)	0.2694	6.874(-2)	6.626(-5)	6.375(-5)	8.573(-5)	0.8227	0.8382	-1.187(-2)	0.4140
				$M/R = 0.16$ vs. 0.16, $\bar{M}_{\rm B} = 0.1600$ vs. 0.1600							
4.263	2.858	5.643(-2)	0.2934	9.499(-2)	2.404(-5)	4.283(-5)	4.043(-5)	0.9863	0.9903	-3.097(-4)	0.9689
3.653	2.452	7.007(-2)	0.2931	8.988(-2)	2.093(-5)	3.718(-5)	3.456(-5)	0.9786	0.9833	-6.159(-4)	0.9468
3.044	2.037	9.028(-2)	0.2927	8.461(-2)	1.544(-5)	2.709(-5)	2.441(-5)	0.9621	0.9679	-1.548(-3)	0.8975
2.739	1.821	1.044(-1)	0.2924	8.194(-2)	1.117(-5)	1.921(-5)	1.659(-5)	0.9454	0.9522	-2.795(-3)	0.8464
2.556	1.684	1.147(-1)	0.2922	8.036(-2)	1.693(-5)	1.689(-5)	1.253(-5)	0.9291	0.9368	-4.126(-3)	0.7937
2.434	1.585	1.227(-1)	0.2921	7.933(-2)	1.539(-5)	2.183(-5)	1.667(-5)	0.9127	0.9213	-5.743(-3)	0.7351
2.312	1.478	1.316(-1)	0.2920	7.833(-2)	1.866(-5)	2.815(-5)	1.727(-5)	0.8876	0.8986	-8.268(-3)	0.6512
2.251	1.405	1.365(-1)	0.2919	7.783(-2)	1.504(-5)	1.274(-5)	2.947(-5)	0.8614	0.8745	-1.052(-2)	0.5389
2.220	1.355	1.390(-1)	0.2919	7.754(-2)	1.168(-4)	1.423(-4)	1.751(-4)	0.8386	0.8535	-1.314(-2)	0.4546
				$M/R = 0.18$ vs. 0.18, $\bar{M}_{\rm B} = 0.1710$ vs. 0.1710							
3.654	2.692	7.173(-2)	0.3106	9.902(-2)	3.784(-5)	6.963(-5)	6.598(-5)	0.9842	0.9887	-6.028(-4)	0.9618
3.044	2.247	9.228(-2)	0.3101	9.334(-2)	3.055(-5)	5.616(-5)	5.218(-5)	0.9728	0.9781	-1.402(-3)	0.9269
2.740	2.018	1.066(-1)	0.3099	9.046(-2)	2.478(-5)	4.546(-5)	4.136(-5)	0.9617	0.9677	-2.408(-3)	0.8923
2.557	1.877	1.170(-1)	0.3097	8.874(-2)	2.091(-5)	3.724(-5)	3.304(-5)	0.9513	0.9579	-3.502(-3)	0.8597
2.313	1.678	1.340(-1)	0.3094	8.650(-2)	2.473(-5)	4.064(-5)	3.310(-5)	0.9287	0.9367	-6.232(-3)	0.7855
2.191	1.570	1.441(-1)	0.3092	8.542(-2)	3.136(-5)	5.104(-5)	3.558(-5)	0.9091	0.9188	-8.975(-3)	0.7201
2.130	1.508	1.497(-1)	0.3092	8.490(-2)	2.370(-5)	3.947(-5)	2.302(-5)	0.8934	0.9044	-1.088(-2)	0.6571
2.099	1.466	1.525(-1)	0.3091	8.461(-2)	1.552(-5)	1.699(-5)	3.932(-5)	0.8783	0.8905	-1.254(-2)	0.5868
2.068	1.411	1.553(-1)	0.3091	8.421(-2)	1.832(-4)	2.664(-4)	3.122(-4)	0.8547	0.8691	-1.612(-2)	0.4960

TABLE IV: Same as Table III but for different mass binary systems. The superscript " ' " denotes the values for the more massive star.

$\bar{d}_G$	$\tilde{d}$	$\bar{\Omega}$	$\bar{M}$	$\bar{J}$	$|VE(\bar{M})|$	$|VE(\bar{GB})|$	$|VE(\bar{FUS})|$	a_2/a_1 a'_2/a'_1	a_3/a_1 a'_3/a'_1	δe_c $\delta e'_c$	χ χ'
					Different mass stars, Irrotational case						
				$M/R = 0.12$ vs. 0.14,	$\bar{M}_B = 0.1299$ vs. 0.1299						
6.090	3.602	3.199(-2)	0.2572	8.790(-2)	1.249(-5)	2.119(-5)	2.011(-5)	0.9904	0.9938	-1.076(-4)	0.9819
								0.9940	0.9964	-5.955(-5)	0.9889
3.653	2.156	6.637(-2)	0.2565	7.191(-2)	8.519(-6)	1.408(-5)	1.267(-5)	0.9586	0.9645	-1.116(-3)	0.8950
								0.9748	0.9789	-5.560(-4)	0.9355
3.044	1.769	8.579(-2)	0.2562	6.751(-2)	5.310(-6)	8.355(-6)	7.043(-6)	0.9212	0.9295	-3.284(-3)	0.7858
								0.9538	0.9591	-1.541(-3)	0.8732
2.861	1.643	9.359(-2)	0.2561	6.619(-2)	8.448(-6)	1.253(-5)	9.948(-6)	0.8985	0.9081	-4.941(-3)	0.7131
								0.9420	0.9480	-2.256(-3)	0.8374
2.739	1.553	9.949(-2)	0.2560	6.533(-2)	1.412(-5)	1.903(-5)	1.371(-5)	0.8750	0.8867	-6.731(-3)	0.6375
								0.9311	0.9379	-2.988(-3)	0.8038
2.677	1.503	1.027(-1)	0.2559	6.490(-2)	1.371(-5)	1.827(-5)	1.285(-5)	0.8583	0.8712	-7.965(-3)	0.5768
								0.9243	0.9316	-3.465(-3)	0.7824
2.616	1.446	1.061(-1)	0.2559	6.448(-2)	9.790(-6)	1.443(-5)	8.245(-6)	0.8333	0.8481	-9.742(-3)	0.4796
								0.9163	0.9242	-4.057(-3)	0.7563
2.585	1.412	1.079(-1)	0.2559	6.428(-2)	6.266(-7)	5.076(-6)	3.032(-6)	0.8146	0.8308	-1.118(-2)	0.4100
								0.9115	0.9197	-4.414(-3)	0.7404
				$M/R = 0.14$ vs. 0.16,	$\bar{M}_B = 0.1461$ vs. 0.1600						
4.872	3.125	4.591(-2)	0.2822	9.348(-2)	2.010(-5)	3.534(-5)	3.351(-5)	0.9865	0.9907	-2.313(-4)	0.9714
								0.9913	0.9944	-1.466(-4)	0.9819
3.653	2.346	6.896(-2)	0.2817	8.401(-2)	1.587(-5)	2.772(-5)	2.558(-5)	0.9691	0.9746	-8.582(-4)	0.9225
								0.9805	0.9846	-5.065(-4)	0.9509
3.044	1.941	8.893(-2)	0.2813	7.901(-2)	1.123(-5)	1.927(-5)	1.713(-5)	0.9436	0.9507	-2.314(-3)	0.8477
								0.9653	0.9703	-1.292(-3)	0.9052
2.739	1.726	1.029(-1)	0.2810	7.650(-2)	1.417(-5)	2.285(-5)	1.876(-5)	0.9161	0.9249	-4.405(-3)	0.7630
								0.9498	0.9558	-2.366(-3)	0.8577
2.617	1.634	1.096(-1)	0.2809	7.551(-2)	1.342(-5)	2.021(-5)	1.619(-5)	0.8974	0.9072	-5.894(-3)	0.6942
								0.9405	0.9470	-3.135(-3)	0.8285
2.495	1.534	1.171(-1)	0.2808	7.454(-2)	1.867(-5)	2.751(-5)	1.896(-5)	0.8692	0.8817	-8.357(-3)	0.6020
								0.9278	0.9353	-4.218(-3)	0.7882
2.434	1.472	1.211(-1)	0.2808	7.406(-2)	6.809(-6)	1.456(-5)	4.008(-6)	0.8423	0.8569	-1.046(-2)	0.4925
								0.9195	0.9276	-4.967(-3)	0.7611
2.403	1.434	1.232(-1)	0.2808	7.382(-2)	2.180(-5)	1.778(-5)	3.298(-5)	0.8210	0.8372	-1.249(-2)	0.4165
								0.9146	0.9230	-5.427(-3)	0.7442
				$M/R = 0.16$ vs. 0.18,	$\bar{M}_B = 0.1600$ vs. 0.1710						
4.263	2.988	5.713(-2)	0.3022	9.963(-2)	3.261(-5)	5.931(-5)	5.653(-5)	0.9853	0.9897	-3.607(-4)	0.9671
								0.9904	0.9939	-2.793(-4)	0.9789
3.044	2.136	9.130(-2)	0.3014	8.885(-2)	2.260(-5)	4.105(-5)	3.774(-5)	0.9597	0.9660	-1.765(-3)	0.8917
								0.9745	0.9793	-1.225(-3)	0.9308
2.618	1.821	1.123(-1)	0.3010	8.498(-2)	1.484(-5)	2.691(-5)	2.391(-5)	0.9312	0.9393	-4.138(-3)	0.8036
								0.9578	0.9636	-2.732(-3)	0.8786
2.435	1.676	1.239(-1)	0.3008	8.336(-2)	3.135(-5)	5.044(-5)	3.855(-5)	0.9072	0.9171	-6.569(-3)	0.7268
								0.9448	0.9516	-4.189(-3)	0.8376
2.312	1.568	1.328(-1)	0.3007	8.230(-2)	2.650(-5)	4.263(-5)	2.981(-5)	0.8791	0.8912	-9.320(-3)	0.6225
								0.9323	0.9400	-5.731(-3)	0.7972
2.282	1.536	1.352(-1)	0.3007	8.204(-2)	1.853(-5)	3.204(-5)	1.787(-5)	0.8661	0.8793	-1.047(-2)	0.5663
								0.9284	0.9363	-6.185(-3)	0.7842
2.251	1.498	1.377(-1)	0.3006	8.177(-2)	1.672(-5)	1.483(-5)	3.366(-5)	0.8461	0.8609	-1.245(-2)	0.4852
								0.9240	0.9322	-6.763(-3)	0.7692
2.233	1.473	1.392(-1)	0.3006	8.159(-2)	6.054(-5)	7.237(-5)	9.823(-5)	0.8318	0.8478	-1.447(-2)	0.4392
								0.9210	0.9294	-7.143(-3)	0.7589